Electric-Potential-Induced Complete Control of Magnetization in MnZnSb Metallic Ferromagnets

*Martin Møller Greve, Bijoy Das, Ibrahim Issac, Ralf Witte, Di Wang, Robert Kruk, Horst Hahn, and Subho Dasgupta**

Magnetoelectric coupling refers to electric-field control of magnetism, which may offer low-power memory and beyond-CMOS electronics. However, contenders of magnetic phase change materials, such as the dilute magnetic semiconductors (DMS), show weak ferromagnetism whereas the ultra-small screening lengths of robust metallic magnets in artificially stacked thin film heterostructures reduce the extent of controllable magnetization to sub-atomic distances, thereby diminishing the sheer magnitude of the tunable magnetization. In contrast, an electrochemical control of magnetization has recently been proposed where reversible electrochemistry/ion-exchange is used to control magnetism in bulk ferromagnets. However, so far, ionic control of magnetism is limited to spinel ferrites and highly correlated oxide systems. Here, it is reported that the ionic control of magnetism can be extended to metallic ferromagnets; complete and reversible switching of ferromagnetism is demonstrated in bulk MnZnSb intermetallic compounds at room temperature. An electrochemically controlled reversible tuning of magnetization across the magnetic phase transition temperature is demonstrated. The observed phenomenon can be explained by the distortion of the crystal lattice, upon Li-ion insertion into the MnZnSb interstitial sites, accompanied by a change in the magnetic moment of the manganese ions; acting together, both these effects lead to the collapse of the ferromagnetic order in MnZnSb.

1. Introduction

The breakthrough in digital electronics, information, and communication technology is largely due to the existence of semiconductor materials, such as silicon, with matching electron and hole mobility, thereby ensuring viability of the CMOS technologies. However, unfortunately this is not the case with magnetic semiconductors, which limit the possibility of developing practical and commercially relevant spintronic devices. Although DMS systems, such as $Mn_{0.05}Ge_{0.95}$ quantum dots have shown ferromagnetic order and magnetoelectric tuning at room temperature,[1,2] the measured magnetic moment in the system has not been large, less than $1/10^{th}$ of μ_B (Bohr Magnetron) per formula unit. On the other hand, in case of strong metallic magnets, extreme nanostructuring is required to obtain any measureable change in magnetization. The reason being the small mean field screening length in metals, which conventionally can be computed from the Fermi energy ε_F as[3] $\lambda_D = \sqrt{\varepsilon_F/4\pi n_e e^2}$. However, this formula, in case of metals, with $n_e = 8.5 \times 10^{22}$ cm^{-3} (e.g., for copper), results in an unrealistic screening length of 0.55 Å. The inference that can be drawn here is that while the Thomas–Fermi screening length approximation works well for semiconductors, however, it breaks down for metals. Later, calculations from Lang and Kohn,[4] and Kempa[5] using hydrodynamic approximation have shown that the mean field penetration within a metal surface may actually be of the order of 0.25–0.3 nm. Nonetheless, such dimensions are also less than a monolayer thickness of metal atoms in most cases. Consequently, electric field control has typically been limited to surface layer of atoms in best reports on magnetoelectric systems.[6–8] While, only 2–4% change in coercivity has been recorded for few nanometer thick FePt and FePd films,[6] Chiba et al. have shown electric field controlled complete ferro-to-paramagnetic transition at 321 K for 0.4 nm cobalt thin films.[7] Thus, it may be noted that electric field

Dr. M. M. Greve, Dr. B. Das, Dr. I. Issac, Dr. R. Witte, Dr. D. Wang, Dr. R. Kruk, Prof. H. Hahn, Prof. S. Dasgupta
Institute for Nanotechnology
Karlsruhe Institute of Technology (KIT)
Eggenstein-Leopoldshafen D-76344, Germany
E-mail: dasgupta@iisc.ac.in

Dr. M. M. Greve
Department of physics and technology
University of Bergen
Bergen 5007, Norway

Dr. B. Das
Centre for Automotive Energy Materials
International Advanced Research Centre for Powder Metallurgy and New Materials (ARCI)
Chennai, India

Dr. D. Wang
Karlsruhe Nano Micro Facility
Karlsruhe Institute of Technology (KIT)
Eggenstein-Leopoldshafen D-76344, Germany

Prof. S. Dasgupta
Department of Materials Engineering
Indian Institute of Science
C V Raman Avenue
Bangalore 560013, India

control of magnetization is possible in metals, however, only for an extremely small magnetic (volume and therefore) signal.

In contrast, an ionic control of magnetization has recently been proposed, where reversible electrochemistry (either a surface adsorption or a bulk insertion of ions) has been used to control the magnetic state of materials.[9–17] Reversible ion insertion or surface chemisorption is naturally a stronger tool to alter the physical states of a material; for instance, in case of pseudocapacitors, the accumulated surface charge density can be orders of magnitude larger than the purely non-Faradaic, electrostatic electric double layer capacitance (EDLC).[9] On the other hand, the inserted ionic species in a magnetic metal-oxide system may change the oxidation state of the metal cation[10] and also strongly vary the bond length and bond angle of the interacting ions.[11] In this context, it is interesting to note that the reports on ionic control of magnetism are mostly limited to insulating or semiconducting oxides[9–15] (spinel ferrites and highly correlated electronic systems); whereas, the work on ionic control in metallic magnets has again been limited to ultrathin (0.9 nm Co) films only.[16,17] Therefore, it may be stated that reports on either electrostatic or electrochemical (ionic) control of magnetization in metallic magnets (involving 3d/4f metals) have been limited to ultra-thin films and an external control over magnetization in bulk volume of metallic magnets has not been reported in the literature. In this regard, here we demonstrate that a complete control over magnetic state is possible in intermetallic compound manganese zinc antimony MnZnSb (MZS) in bulk. MnZnSb crystalizes in a tetragonal Cu_2Sb-type crystal structure (space group P4/mmm);[18] in fact, MZS is an ordered structure, where Mn atoms occupy the c-plane of the tetragonal layered position and Zn and Sb atoms form two nonmagnetic layers that separate the magnetic Mn layers. In the parent Mn_2Sb compound, the Sb atoms are trivalent and therefore Mn atoms are monovalent (Mn-I) and divalent (Mn-II). In MnZnSb structure, the divalent Zn replaces the divalent Mn (Mn-II), and hence only the monovalent Mn (Mn-I) remains.[19] While, Mn_2Sb possesses a transition temperature above 550 °C,[20,21] the T_C for MnZnSb lowers to just above room temperature; moreover, a sharp phase transition is typically observed, thereby making it an ideal system for ion-controlled magnetization tuning.

The experimental approach in this study has been essentially similar to our previous publications.[10,11] An in situ Li-ion battery cell has been prepared with intermetallic MnZnSb as the cathode material and pure Li metal as anode. The ideal potential window for the reversible electrochemistry has been identified. Subsequently, ex situ and in situ magnetometry measurements with respect to electrochemical Li intercalation/de-intercalation have been carried out. The most intriguing feature of the present work is that the magnetization MnZnSb can be completely annihilated upon lithiation and then fully recovered, once the material is delithiated to its open cell voltage. In fact, a complete control over the measured magnetization has been observed, presumably for the first time in bulk volume of metallic magnets.

2. Results and Discussion

In order to facilitate easy comparison between the discharged (lithiated) samples and the as-prepared ones, the structural, chemical, and morphological characterizations of the as-prepared MnZnSb have been carried out with powders collected from the electrode of the fabricated electrochemical cell. It has been determined that a potential window from the open circuit voltage (around 2.8 to 3 V versus Li/Li^+) down to a discharge potential of 0.57 V (versus Li/Li^+) can be chosen for the reversible electrochemistry that would allow the associated physical properties (for example, magnetization in this case) to vary reversibly as well. The high-resolution X-ray diffraction (XRD) pattern of the as-prepared and lithiated MnZnSb is shown in **Figure 1**a. As can be seen, all the major reflections could be identified as resulting either from MnZnSb (JCPDS data 152–7599) or graphite (JCPDS data 900-0046). However, there are still a few minor reflections that cannot be indexed, for example between the major peaks at $2\theta = 33.58°$ and 42.18°. Next, a schematic structure of the tetragonal MnZnSb crystal is shown in Figure 1b. It can be noted that the in-plane manganese atoms are separated by the nonmagnetic Sb and Zn atoms in MnZnSb. In addition to the un-indexed reflections in the XRD pattern, the chemical analysis performed using energy dispersive X-ray spectroscopy at many different locations also results in Mn:Zn:Sb ratios which are not exactly stochiometric (one-third for each element); in fact the data collected over a larger area (thereby averaging out local inhomogeneities) indicate typically a lower Zn content (as is shown in the representative images in Figure 1c). The lower Zn content increases the possibility of having a minor fraction of a manganese-antimony rich secondary phase. Here, it may be noted that the transition temperature of binary Mn_2Sb and MnSb are 550 K[20,21] and 587,[22] respectively, and the saturation magnetization of these systems is also much higher than MnZnSb, more than 100 $Am^2\ kg^{-1}$, in each case. Therefore, the existence of such a binary compound should actually be easy to detect with magnetic measurements, and in fact, it has been possible to confirm their presence as will be discussed in the next sections. Next, scanning electron micrographs are shown for as-prepared powder (Figure 1d), as-prepared electrochemical cell electrode (Figure 1e), and discharged (lithiated) cell electrode (Figure 1f), respectively. As per expectation, no significant morphological change can be noted with the lithium intercalation process.

Figure 2a explains the selection of the discharge potential as 0.57 V (versus Li/Li^+). The cyclovoltammogram performed using a standard Swagelok cell for the potential window between the open circuit voltage (OCV) and 0 V, at a constant scan speed of 50 $\mu V\ s^{-1}$ shows a small intercalation peak around 0.65–0.7 V (again quite expected potential region for Li intercalation in metal alloys) followed by a substantially stronger current peak, which is associated with complete structural destruction of the parent electrode compound and formation of LiZn and Li_3Sb alloys. It has been noted that when a potential limit for the discharge process is chosen as 0.57 V (versus Li/Li^+), just after the first Li intercalation peak, the lithiation/delithiation process and associated change in physical properties can be highly reversible, without involving an irreversible structural change in the parent electrode material (Figure 1a). Next, the in situ magnetic measurements have been carried out with simultaneous galvanostatic discharge–charge processes with a constant current of 60 $mA\ g^{-1}$ (Figure 2b). The in situ measurement data have been recorded for about 10 h,

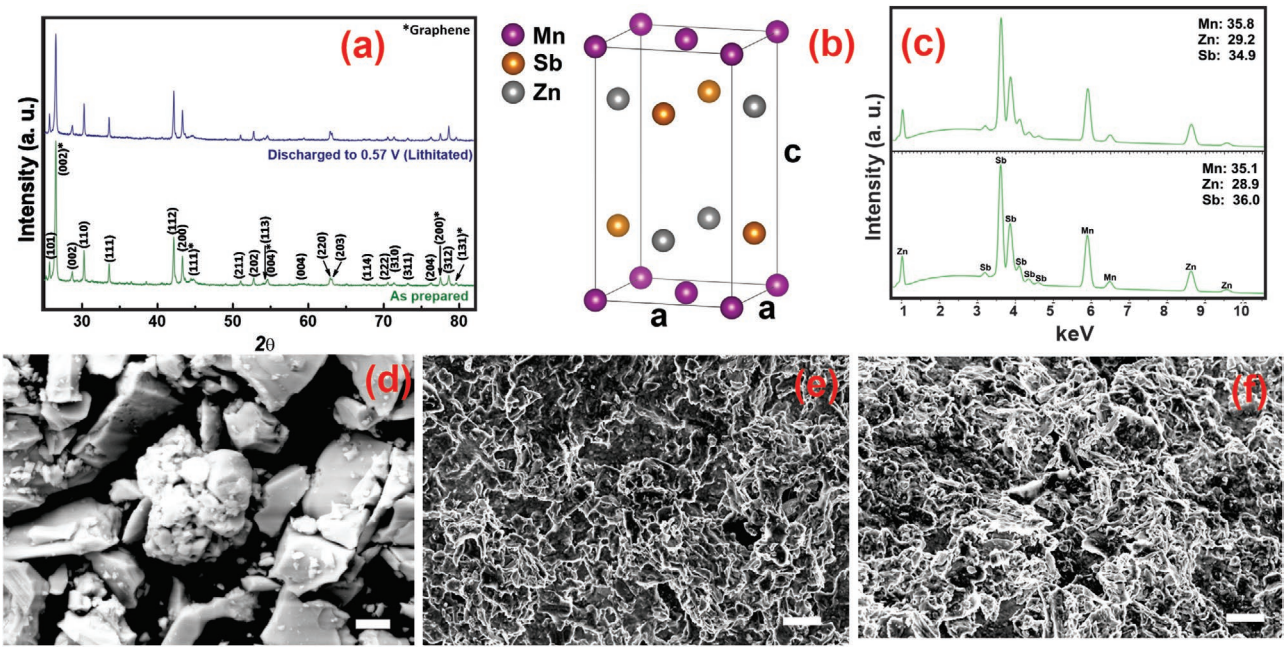

Figure 1. a) High-resolution X-ray diffraction pattern of MnZnSb, as-prepared and lithiated (discharged) to 0.57 V (versus Li/Li$^+$). b) Schematic representation of the MnZnSb crystal structure. c) EDX spectroscopy of as-prepared MnZnSb taken over two large areas of dispersed powders so as to provide elemental analysis for the bulk amount of sample. Elements other than Mn, Zn, Sb are eliminated and an elemental ratio of the three primary constituents has been obtained. d) SEM image of the as-prepared MnZnSb. e) SEM image of the as-prepared battery electrode (admixed with graphene nanoparticles and PVDF). f) SEM image of the electrode after discharged (lithiated) to 0.57 V (versus Li/Li$^+$). The scale bar is 4 μm in (d) and it is 20 μm in (e,f).

after which the electrical contact (with the sample) was lost due to the unavoidable and extensive movement of the electrochemical cell in the magnetic field for the magnetization measurements. However, to point out the high electrochemical reversibility many charging–discharging cycles were measured ex situ, which will be presented next. The in situ measurement shown in Figure 2b has been performed with a small applied field of 1000 Oe. The measured variation in magnetization ranges from 25 Am^2 kg^{-1} for the as-prepared electrode to about 5 Am^2 kg^{-1} for the discharged (lithiated) one, corresponding to a reduction in magnetization of about 80%. However, the remaining unaltered magnetism may largely be due to the spurious and strongly magnetic second phase.

Furthermore, ex situ measurements have also been carried to ensure complete reversibility of the magnetic response. **Figure 3** shows the hysteresis and field-cooled (fc)-zero

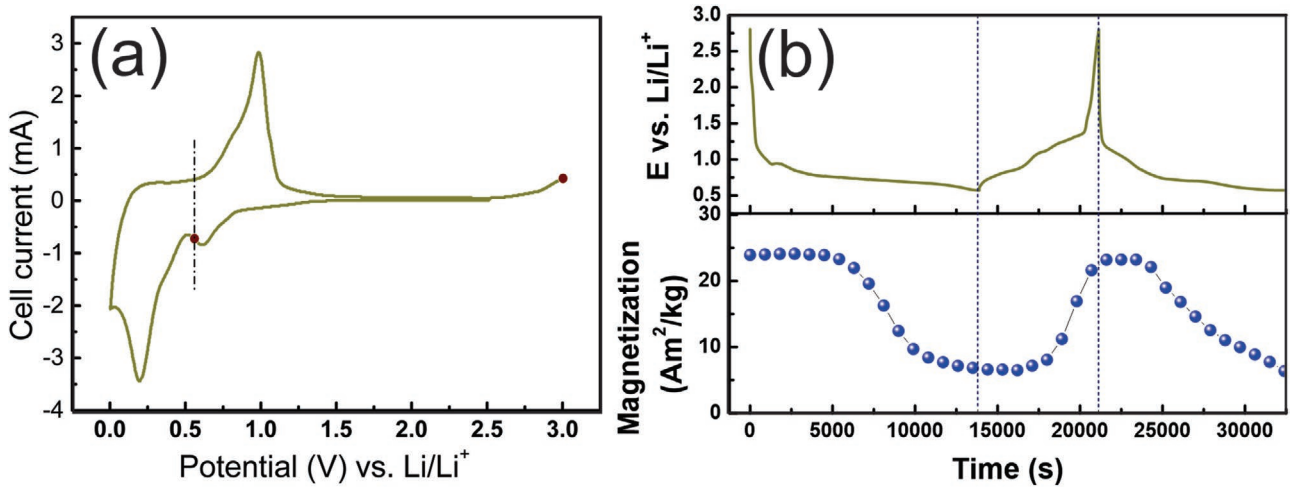

Figure 2. a) The cyclovoltammogram of the MnZnSb electrode versus Li/Li$^+$. The open circuit voltage (OCV) and the chosen limit of the discharge potential are shown with maroon dots. b) The in situ magnetic measurements, while performing the electrochemical lithiation–delithiation cycles. The discharge (lithiation) and charge (delithiation) potential limits are shown with dotted lines. The discharge–charge process used a constant current of 60 mA g^{-1}, whereas a constant magnetic field of 1000 Oe was used.

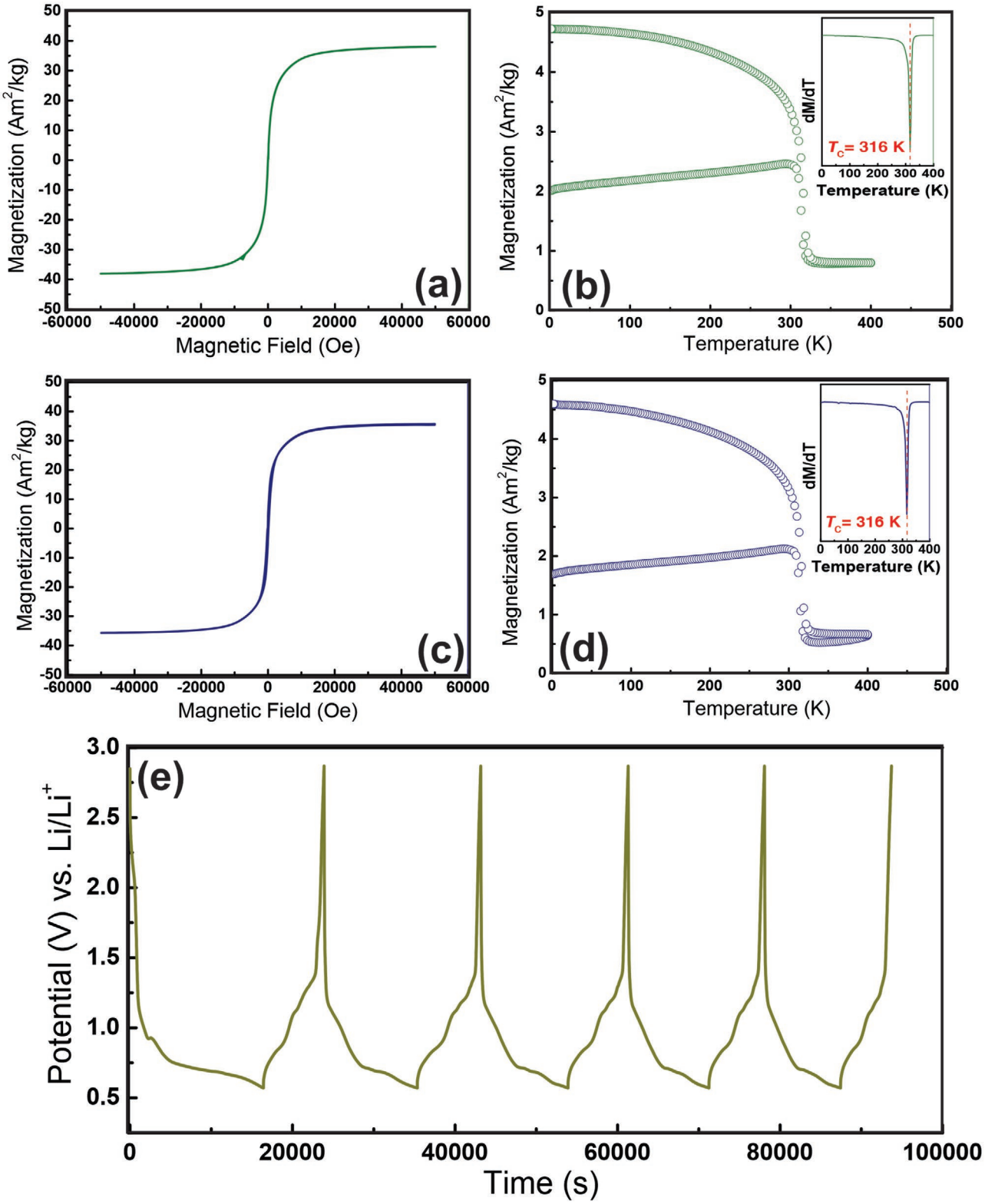

Figure 3. a) Magnetic hysteresis of the as-prepared MnZnSb battery electrode, measured at 300 K. b) The field-cooled (fc)- zero field-cooled (zfc) curves of the same electrode, measured with an applied magnetic field of 100 Oe; the derivative of the magnetization with respect to temperature determines the transition temperature to be 316 K (inset). c) The magnetic hysteresis of the MnZnSb electrode, after five complete discharge–charge cycles, measured at 300 K. d) The field-cooled (fc)- zfc curves of the electrode, after five discharge–charge cycles, which also have resulted in an absolutely identical Curie temperature (inset). e) The electrochemical data of the associated discharge–charge cycles.

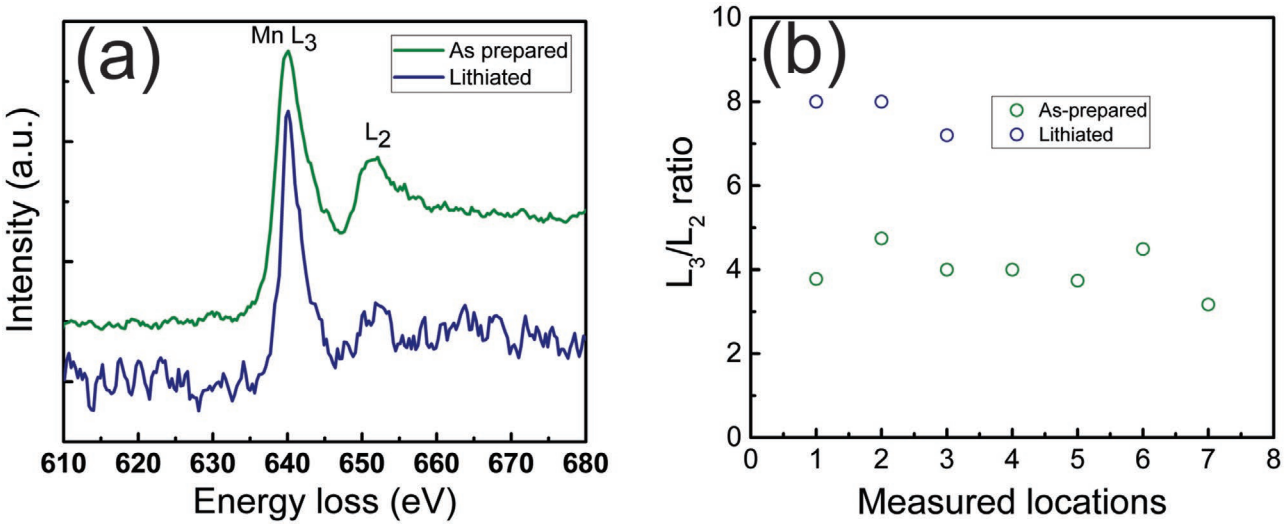

Figure 4. a) Comparison of average electron energy loss spectroscopy (EELS) spectra that are recorded at different locations of the as-prepared and lithiated MnZnSb sample. b) The measured data show Mn- L_3/L_2 ratio at different locations for the as-prepared and lithiated MnZnSb electrode material.

field-cooled (zfc) magnetization curves of the as-prepared (Figure 3a,b) MnZnSb electrode and MnZnSb electrode at the fully charged (delithiated) state after five complete discharge–charge cycles (Figure 3c,d), respectively. Figure 3e shows the corresponding electrochemical data of the discharge–charge processes. The amount of intercalated Li has been calculated here from the second discharge cycle (the first one usually involves solid electrolyte interface formation and may result in an erroneous value) to be around 1.67 moles of Li^+ per formula unit of MZS intermetallic. First, from the fc-zfc curves of the as-prepared and the five times complete cycled MnZnSb samples, an extremely high reversibility in the measured saturation magnetization and extracted transition temperature values can be noted. The observed magnetic transition temperature (316 K) is found to be identical to the values reported in the literature (310–325 K).[18,19,23,24] However, it may also be noted that a noticeable fraction of magnetization remains intact even above the magnetic transition temperature (Figure 3b,d); the constant (with respect to temperature) value of the residual magnetization clearly indicates the presence of a second magnetic phase with much higher Curie temperature. In this regard, an exactly identical observation, that is the presence of a constant residual magnetization after the Curie temperature has been reported by Johnson and Jeitschko in a mixture of phases with predominantly MnZnSb and a small fraction of Mn_2Sb phase.[19] It may be noted that the quantitative value of magnetization with higher transition temperature may actually be about 20–25% of the total magnetization measured at 300 K. In this regard, the saturation magnetization of about 40 $Am^2\ kg^{-1}$ measured for MnZnSb at 300 K is also substantially higher than the magnetization measured at 4.2 K (1.2–1.5 μ_B per manganese atom) in earlier reports.[19,23] All of these experimental evidences confirm the presence of a second phase in as-synthesized MnZnSb; consequently, it may be safe to claim that an electrochemically driven reversible and complete transformation across the magnetic transition temperature of the MnZnSb fraction has been achieved in the present case (Figure 2b). In other words, although often challenging due to a common tendency of phase separation in this tertiary alloy systems,[19] a successful synthesis of a completely phase-pure MnZnSb may actually demonstrate a clearer transition across the Curie temperature; i.e., a reversible and complete ferro-to-paramagnetic transition in bulk metallic ferromagnets. Nonetheless, even though a complete 100% transformation could not be experimentally demonstrated, the present results can be considered as the proof of principle demonstration of a reversible ion-exchange mediated control of magnetization in bulk volume of ferromagnetic metals.

Next, attempts have been made to determine the underlying mechanism for the On/Off magnetization switching at room temperature. An insertion of the Li ion into the electrode is necessarily accompanied by a chemical reduction of MZS. In order to demonstrate the fact, electron energy loss spectroscopy (EELS) has been performed on the as-prepared and discharged (lithiated) electrode material. Again, the samples are prepared inside an Ar-filled glove box, and are transferred to the transmission electron microscope (TEM) without exposing the samples to ambient conditions using a Gatan 648 vacuum transfer holder. The EELS measurement of Mn $L_{2,3}$ edge for the as-prepared MnZnSb sample shows a L_3/L_2 ratio of about 4, whereas for the lithiated one, most of the measured L_3/L_2 ratio from Mn $L_{2,3}$ edge in different areas have exhibited a ratio larger than 4, indicating a reduced valence state for Mn (**Figure 4**).[25] In fact, in some areas (not shown in Figure 4b), the L_2 intensity has even been close to zero. This clearly indicates a chemical reduction of the magnetic cation, manganese, upon lithiation.[25,26]

In the present study, there may be three possible reasons for the disappearance of the magnetization during the Li insertion: the first one could be the lowering of the value of magnetic exchange integral and associated reduction in ferromagnetic transition temperature, *T*c well below room temperature; the second one could be triggering of the complete transition from the ferromagnetic ground state to the paramagnetic one; and the last possibility would be a direct transition from ferromagnetic

to antiferromagnetic state. Any of these cases has to be related to the presence of the Li-ion in the MZS lattice and/or chemical reduction of Mn in MnZnSb. The crystal structure of MZS clearly shows the layered character, where Mn planes are interspersed with the nonmagnetic ZnSb ones (Figure 1b). This atomic arrangement determines the ground magnetic state, with quasi two-dimensional magnetism. Thus, there is a pronounced two-dimensional character of the ferromagnetic Mn–Mn exchange interactions in the Mn plane (Figure 1b). As a matter of fact, the distance between the in-plane Mn nearest neighbors is critical for the stabilization of the magnetic ground state; be it either ferromagnetic or antiferromagnetic. In this regard, there has been a body of experimental evidence that above a certain critical Mn–Mn nearest neighbor distances, the coupling between intralayer Mn ions switches from ferromagnetic to antiferromagnetic. For example, MnGaGe,[27] MnAlGe,[28] and MnZnSb with smaller Mn–Mn distances are ferromagnetic whereas MnRbSb, MnCsAs, and MnCsSb[29] featuring lengthier in-plane bonds show antiferromagnetic coupling. On the other hand, experiments to investigate the dependence of the magnetic state to pressure have concluded that the *Tc* temperature is also sensitive to the distance between the atomic planes via the indirect superexchange Mn-diamagnetic ion-Mn interactions.[30] Thus, the plausible mechanism behind the disappearance of ferromagnetism could be linked to the Li-ions being positioned exactly between the Mn–Mn layers, in fact, there are many empty interstitial sites that the intercalated Li-ions can occupy, and thereby stretch the MZS lattice. In an extreme case, the in-plane lattice constant "*a*," determining the intraplane Mn–Mn distance, can reach a critical value beyond which the ferromagnetic ground state of MZS switches to an antiferromagnetic one. This kind of crystallographically driven ferro-antiferromagnetic transition mechanism can be supported by the reported observations with similar compounds which are antiferromagnetic and show much larger and more localized Mn magnetic moment.[29] In our case, one can envision a synergetic effect of the incoming electron that reduces the Mn ions, prompting its transition to the more localized electronic state with the higher magnetic moment, and pushing the Mn sublattice toward antiferromagnetic interactions. An alternative scenario, also related to the Li-ion intercalation is that the ferro-to-paramagnetic transition temperature (*Tc*) may simply be lowered due to the stretching of the crystal lattice along the *c* axis (Figure 1b); this would weaken the interplanar superexchange interactions and consequently lower the ferro- to paramagnetic transition temperature.[30]

3. Conclusion

Complete and reversible control of magnetization has been demonstrated in bulk volume of metallic magnets. In the MnZnSb intermetallic system, Li intercalation-driven complete On-and-Off magnetic switching has been observed. The demonstrated On-and-Off magnetic switching may have resulted from a lowering of the ferromagnetic transition temperature of MnZnSb as the crystal stretching along the *c* axis (which is certainly a possibility with Li intercalation at the interstitial cites) would result in a lowering of ferro-to-paramagnetic transition temperature (*Tc*). This may be represented as lowering of the magnetic exchange integral which would eventually lower the transition temperature. The switching effect may also be related to a possible strain/MZS lattice stretching (along the Mn a-plane) and simultaneous chemical reduction of Mn, which together could trigger the direct transition from a ferromagnetic to an antiferromagnetic state. The governing mechanism that is dominating the magnetic transition can be better understood from neutron diffraction experiments revealing the structural changes and magnetic order associated with the Li intercalation in the layered MnZnSb intermetallic system. The present results open up wider possibilities of using robust metallic magnets for complete and reversible magnetization tuning experiments and a large domain of application possibilities that may be exploited in near future.

4. Experimental Section

Synthesis of MnZnSb: The MnZnSb was synthesized using B_2O_3 flux method. All the metal powders were procured from Alfa Aesar; antimony 99.5% (200 mesh); Manganese 99.8% (325 mesh); Zinc 99.9% (100 mesh), and B_2O_3 99%. The metal powders were mixed in equi-atomic ratio and ground to make homogeneous solid mixture then transferred to an alumina crucible. This was followed by an addition of B_2O_3 powder as a flux in 1:1 weight ratio and compacted. The crucible was then placed inside a silica tube and heated to 600 °C for 16 h with a heating rate of 5 °C min^{-1} under a continuous flow of argon with a rate of 50 mL min^{-1}. During the heat treatment the B_2O_3 flux melts serve as a liquid-seal on the top of the metal mixture. This prevents heat dissipation, the sublimation, and oxidation of the alloy. After the heat treatment, the intermetallic alloy was allowed to cool to room temperature and then transferred to the glove box under argon atmosphere and ground to fine particles. The MZS nanopowders thus produced and the lithiated MZS were always handled inside glove box for battery electrode/cell preparation lithiated sample collection, and sample preparation for all structural and microstructural characterizations.

Electrochemical In Situ Cell Preparation: The as-prepared MZS powder was further ground by low energy ball milling, and then mixed with graphene nanoparticles and polyvinylidene fluoride (PVDF) at a weight ratio of 60:30:10. The added graphene ensures superior electrical conductivity and PVDF serves as the binding material. Next, a few drops of *N*-methyl-2-pyrrolidone (NMP) were added to this mixture to form a slurry, which was then coated onto a 15 µm aluminum foil (served as current collector) using doctor blade technique to result in an electrode thickness of 50 µm. Pure lithium metal was used as anode alongside Celgard polypropylene oxide/polyethylene oxide/polypropylene oxide (PPO/PEO/PPO) triblock copolymer membrane separator and Selectilyte LP 30 (1 molar lithium hexafluorophosphate, $LiPF_6$) dissolved in (1:1 w/w) ethylene carbonate (EC) and dimethyl carbonate (DMC) solvents) as the electrolyte (BASF GmbH). During initial electrochemical characterization standard Swagelok-type cell was used; however, later for in situ measurements an indigenously designed electrochemical cell was used that fits within the limited space inside a magnetometer, in this case the size of the electrodes was not larger than 4×4 mm^2. The cells were assembled inside an argon glovebox ($H_2O < 0.5$ ppm; $O_2 < 0.5$ ppm).

Structural and Microstructural Characterization: Intermetallic powders from as-prepared and lithiated electrodes were collected inside the glove box for structural characterizations. High resolution X-ray diffraction was carried out using a STOE STADI P diffractometer (Cu-K_α radiation, Germanium monochromator, Debye–Scherrer geometry, Mythen 1K detector) in sealed glass capillaries. Scanning electron micrographs were obtained using a LEO 1530 Gemini scanning electron microscope at 10 kV acceleration voltage. The EDX spectra were acquired using a

20 kV acceleration voltage and the X-ray signal was detected using an Oxford EDX detector in the same SEM microscope and analyzed with the Aztec software. In order to determine the electronic state of the as-prepared and lithiated MnZnSb, EELS measurements were conducted using a FEI Titan 80–300 TEM operated at 300 kV, and equipped with a Tredium Gatan image filter (GIF).

Electrochemical and Magnetic Measurements: In case of the ex situ electrochemical measurements, galvanostatic charge–discharge cycling and the cyclic voltammetry (CV) measurements were carried out on Swagelok cells, using multichannel battery tester Arbin BT 2000 and Biologic VMP3 potentiostat, respectively. During the CV measurements the cells were cycled at a constant potential scan rate of 50 $\mu V\ s^{-1}$; whereas the galvanostatic charge–discharge cycles were carried out at a constant current density of 60 $mA\ g^{-1}$. The galvanostatic discharge–charge cycles during the in situ measurements were carried out using a Metrohm Autolab 302N potentiostat/galvanostat; again the measurements were performed with a constant current of 60 $mA\ g^{-1}$. The magnetic measurements were carried out using a physical property measurement system (PPMS) from Quantum Design.

Acknowledgements

H.H. and S.D. would like to thank the financial support from Deutsche Forschungsgemeinschaft (DFG) for grants HA 1344/34-1, DA 1781/1-1, respectively.

Conflict of Interest

The authors declare no conflict of interest.

Keywords

ferromagnetism, li-ion intercalation, magnetic switching, magneto-electric coupling, reversible electrochemistry

[1] F. Xiu, Y. Wang, J. Kim, A. Hong, J. Tang, A. P. Jacob, J. Zou, K. L. Wang, *Nat. Mater.* **2010**, *9*, 337.
[2] F. Xiu, Y. Wang, J. Kim, P. Upadhyaya, Y. Zhou, X. Kou, W. Han, R. K. Kawakami, J. Zou, K. L. Wang, *ACS Nano* **2010**, *4*, 4948.
[3] C. Kittel, *Introduction to Solid State Physics*, 8th ed., Wiley, Weinheim, Germany **2004**, p. 405.
[4] N. D. Lang, W. Kohn, *Phys. Rev. B* **1971**, *3*, 1215.
[5] K. Kempa, *Surf. Sci.* **1985**, *157*, L323.
[6] M. Weisheit, S. Fähler, A. Marty, Y. Souche, C. Poinsignon, D. Givord, *Science* **2007**, *315*, 349.
[7] D. Chiba, S. Fukami, K. Shimamura, N. Ishiwata, K. Kobayashi, T. Ono, *Nat. Mater.* **2011**, *10*, 853.
[8] T. Maruyama, Y. Shiota, T. Nozaki, K. Ohta, N. Toda, M. Mizuguchi, A. A. Tulapurkar, T. Shinjo, M. Shiraishi, S. Mizukami, Y. Ando, Y. Suzuki, *Nat. Nanotechnol.* **2009**, *4*, 158.
[9] A. Molinari, P. M. Leufke, C. Reitz, S. Dasgupta, R. Witte, R. Kruk, H. Hahn, *Nat. Commun.* **2017**, *8*, 15339.
[10] S. Dasgupta, B. Das, M. Knapp, R. A. Brand, H. Ehrenberg, R. Kruk, H. Hahn, *Adv. Mater.* **2014**, *26*, 4639.
[11] S. Dasgupta, B. Das, Q. Li, D. Wang, T. T. Baby, S. Indris, M. Knapp, H. Ehrenberg, K. Fink, R. Kruk, H. Hahn, *Adv. Funct. Mater.* **2016**, *26*, 7507.
[12] Q. Zhang, X. Luo, L. Wang, L. Zhang, B. Khalid, J. Gong, H. Wu, *Nano Lett.* **2016**, *16*, 583.
[13] J. Walter, H. Wang, B. Luo, C. D. Frisbie, C. Leighton, *ACS Nano* **2016**, *10*, 7799.
[14] H. B. Li, N. Lu, Q. Zhang, Y. Wang, D. Feng, T. Chen, S. Yang, Z. Duan, Z. Li, Y. Shi, W. Wang, W. H. Wang, K. Jin, H. Liu, J. Ma, L. Gu, C. Nan, P. Yu, *Nat. Commun.* **2017**, *8*, 2156.
[15] X. Zhu, J. Zhou, L. Chen, S. Guo, G. Liu, R. W. Li, W. D. Lu, *Adv. Mater.* **2016**, *28*, 7658.
[16] U. Bauer, L. Yao, A. J. Tan, P. Agrawal, S. Emori, H. L. Tuller, S. Van Dijken, G. S. D. Beach, *Nat. Mater.* **2015**, *14*, 174.
[17] A. J. Tan, M. Huang, C. O. Avci, F. Büttner, M. Mann, W. Hu, C. Mazzoli, S. Wilkins, H. L. Tuller, G. S. D. Beach, *Nat. Mater.* **2019**, *18*, 35.
[18] N. Y. Pankratov, V. I. Mitsiuk, V. M. Ryzhkovskii, S. A. Nikitin, *J. Magn. Magn. Mater.* **2019**, *470*, 46.
[19] V. Johnson, W. Jeitschko, *J. Solid State Chem.* **1977**, *75*, 71.
[20] T. Kanomata, T. Kawashima, T. Kaneko, H. Takahashi, N. Mōrin, *Jpn. J. Appl. Phys.* **1991**, *30*, 541.
[21] M. Suzuki, M. Shirai, K. Motizuki, *J. Phys.: Condens. Matter* **1992**, *4*, L33.
[22] K. Motizuki, *Electronic Structure and Magnetism of 3d-Transitonal Metal Pnictides*, Springer-Verlag,, Berlin Heidelberg, **2007**.
[23] S. Mori, T. Kanomata, H. Yamauchi, S. Sakatsume, T. Kaneko, *Jpn. J. Appl. Phys.* **1993**, *32*, 273.
[24] F. Ono, X. Hu, N. Fujii, K. Hayashi, N. Okada, S. Endo, T. Kanomata, *Phys. B* **1997**, *237–238*, 162.
[25] H. Tan, J. Verbeeck, A. Abakumov, G. Van Tendeloo, *Ultramicroscopy* **2012**, *116*, 24.
[26] A. Kimura, S. Suga, T. Shishidou, S. Imada, T. Muro, *Phys. Rev. B* **1997**, *56*, 6021.
[27] G. B. Street, E. Sawatzky, K. Lee, *J. Appl. Phys.* **1973**, *44*, 410.
[28] S. Mizukami, A. Sakuma, T. Kubota, Y. Kondo, A. Sugihara, T. Miyazaki, *Appl. Phys. Lett.* **2013**, *103*, 142405.
[29] R. Müller, M. Kuckel, H. U. Schuster, P. Müller, W. Bronger, *J. Alloys Compd.* **1991**, *176*, 167.
[30] H. Matsuzaki, S. Endo, Y. Notsu, F. Ono, T. Kanomata, T. Kaneko, *Jpn. J. Appl. Phys.* **1993**, *32*, 271.